Evidence for excitation of two resonance states in the isovector two-baryon system with a mass of 2.2 GeV/ c^2

V. Komarov,[1] D. Tsirkov,[1,*] T. Azaryan,[1] Z. Bagdasarian,[2,3] S. Dymov,[1,2] R. Gebel,[2] B. Gou,[4] A. Kacharava,[2] A. Khoukaz,[5] A. Kulikov,[1] V. Kurbatov,[1] B. Lorentz,[2] G. Macharashvili,[1,3] D. Mchedlishvili,[2,3] S. Merzliakov,[2] S. Mikirtytchiants,[2,6] H. Ohm,[2] M. Papenbrock,[5] F. Rathmann,[2] V. Serdyuk,[2] V. Shmakova,[1] H. Ströher,[2] S. Trusov,[2,7] Yu. Uzikov,[1,8,9] and Yu. Valdau[6,10]

[1]*Laboratory of Nuclear Problems, Joint Institute for Nuclear Research, RU-141980 Dubna, Russia*

[2]*Institut für Kernphysik and Jülich Centre for Hadron Physics, Forschungszentrum Jülich, D-52425 Jülich, Germany*

[3]*High Energy Physics Institute, Tbilisi State University, GE-0186 Tbilisi, Georgia*

[4]*Institute of Modern Physics, Chinese Academy of Sciences, Lanzhou 730000, China*

[5]*Institut für Kernphysik, Universität Münster, D-48149 Münster, Germany*

[6]*High Energy Physics Department, St. Petersburg Nuclear Physics Institute, RU-188350 Gatchina, Russia*

[7]*Skobeltsyn Institute of Nuclear Physics, Lomonosov Moscow State University, RU-119991 Moscow, Russia*

[8]*Department of Physics, Lomonosov Moscow State University, RU-119991 Moscow, Russia*

[9]*Dubna State University, RU-141980 Dubna, Russia*

[10]*Helmholtz-Institut für Strahlen- und Kernphysik, Universität Bonn, D-53115 Bonn, Germany*

(Received 2 September 2015; revised manuscript received 29 March 2016; published 17 June 2016)

We report on measurements of the differential cross section $d\sigma/d\Omega$ and the first measurement of the analyzing power A_y in the $\Delta(1232)$ excitation energy region of the reaction $pp \to \{pp\}_s\pi^0$ where $\{pp\}_s$ is a $^1S_0$ proton pair. The experiment has been performed with the ANKE spectrometer at COSY-Jülich. The data reveal a peak in the energy dependence of the forward $\{pp\}_s$ differential cross section, a minimum at zero degrees of its angular distribution, and a large analyzing power. The results present a direct manifestation of two two-baryon resonance-like states with $J^P = 2^-$ and 0^- and an invariant mass of 2.2 GeV/c^2.

DOI: 10.1103/PhysRevC.93.065206

I. INTRODUCTION

The topic of resonances in two-baryon systems has started to be discussed [1,2] promptly after formulation of the SU(3) flavor symmetry concept. In Ref. [2] a theory of strongly interacting particles classified two-baryon states with hypercharge $Y = 2$ and strangeness $S = 0$ as members of an SU(6) unitary multiplet of states D_{TJ} with isospin T and angular momentum J. The lowest states of the multiplet corresponded to D_{01} for the real deuteron and D_{10} for the virtual singlet deuteron and the $^1S_0$ proton pair. The states D_{12} and D_{03} were predicted as $\Delta(1232)N$ and $\Delta(1232)\Delta(1232)$ resonances, respectively. The term "resonance" was used there in its loosest sense to denote relative enhancement of an interaction cross section at a reasonably-well-defined energy [1] and definite TJ values. Extensive searches for two-baryon resonances started somewhat later and were motivated by the success of the quark-bag models [3,4]. The models reproduced rather well the spectroscopy of the known mesons and baryons and predicted on the same basis the existence of two-baryon resonances. The term "dibaryons" has become strongly bound to such resonances of the compact six-quark structure. In the searches for dibaryons a smallness of their width, $\Gamma \lesssim 100$ MeV, was considered as a distinct signal of their existence.

The only significant result of the experiments aimed to observe dibaryons was the discovery of the $^1D_2$, $^3F_3$, and $^3P_2$ resonances in elastic proton-proton scattering (see Refs. [5–7] and references therein). Here the standard notation $^{2S+1}L_J$ is used for the partial wave with the orbital angular momentum L, spin S, and total angular momentum J. These states meet the strict requirements of being a resonance: proper behavior of the amplitudes in the Argand plot and existence of poles of the S matrix in the complex energy plane [5,6]. However, the position of the poles close to the ΔN branching line led to an established interpretation of the poles as conventional hadron states in the ΔN channel but not dibaryons. At the qualitative level this interpretation is supported by closeness of the resonance energies to a sum of the nucleon and Δ isobar masses and of the resonance widths to the width of a free isobar.

Strong inelasticity of the pp resonances $^1D_2$, $^3F_3$, $^3P_2$ leads to absence of the relevant peaks in the spin-averaged cross sections of the elastic pp scattering. Therefore it is possible to bring out these resonances only via partial-wave analysis (PWA) of a huge amount of data on various spin observables. The resonances are seen much more clearly in processes of a single pion production, where the binary reaction

$$p + p \to d + \pi^+ \tag{1}$$

turned out to be the most informative. Excitation of Δ in the intermediate state of the reaction manifests itself in the form of the well-known intensive peak in the energy dependence of the reaction total cross section [8]. Separation of the peak into its resonance components (Fig. 1) can be done again only via PWA of a great amount of the experimental data [9]. The $^1D_2 p$ transition is determined by the s-wave state of the ΔN two-baryon pair, and the p-wave state is responsible for the $^3F_3 d$ and $^3P_2 d$ transitions (small letters denote the pion wave angular momentum).

*cyrkov@jinr.ru

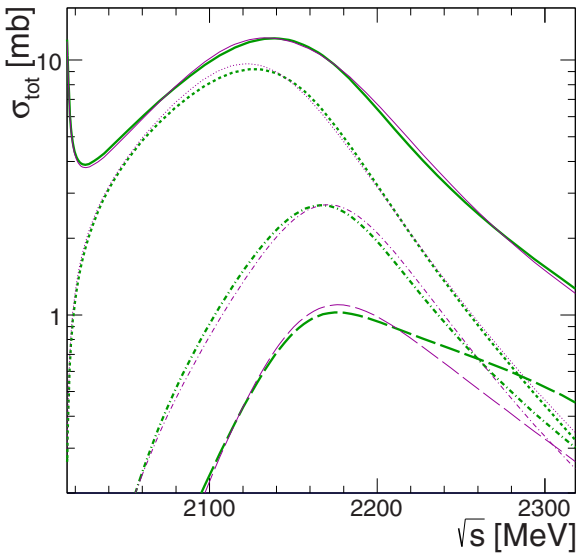

FIG. 1. Contributions of the dominant ^1D_2p (dotted curves), ^3F_3d (dot-dashed curves), and ^3P_2d (dashed curves) amplitudes to the total unpolarized cross section of reaction 1 (solid curves) according to the SAID [10] partial wave analysis. The bold green curves correspond to the C500, and the thin magenta curves correspond to the SP96 solution.

Strict determination of the parameters of the least intensive ^3P_2d transition is complicated by the presence of two close and more intensive transitions. As can be seen from Fig. 1, the shapes of the ^3P_2d peak differ significantly for the C500 and SP96 SAID solutions [10].

It is worth noting that theoretical models based on the traditional meson-baryon approach (see, e.g., Refs. [11–15]) did not succeed either in a detailed description of the polarization observables of reaction (1) in the Δ region, or in an accurate reproduction of the resonance parameters. It may be caused first of all by neglecting a proper description of the intermediate ΔN interaction, but development of the theory [16,17] can probably overcome this difficulty. The principal disadvantage of the traditional meson-baryon approach is disregard of the detailed internal structure of the participating hadrons. This seems important since the crucial distances concerned in the reaction dynamics are comparable with the characteristic hadron size. What may help to overcome this difficulty is development of the "hybrid" models employing the constituent quark structures together with the π- and σ-meson fields [18–21]. These models allow one to explain many features of the NN, $N\Delta$, and $\Delta\Delta$ short-range interaction, but they do not yet provide a systematic and quantitative description of the existing experimental picture.

The experimental study of the two-baryon-system resonances is also far from exhaustive completeness. It is sufficient to recall a recent observation of the isoscalar two-baryon resonance in the energy region of the $\Delta(1232)\Delta(1232)$ excitation [22–24]. The width of this resonance, 70 MeV, is definitely less than the width of a free $\Delta(1232)$ isobar and it stimulated interpretation of the resonance as a genuine dibaryon [25,26].

In the energy region of a single Δ excitation quite new possibilities arise from using the spin-isospin partner of reaction (1),

$$p + p \to \{pp\}_s + \pi^0, \tag{2}$$

where $\{pp\}_s$ denotes a pp pair with an excitation energy less than 3 MeV, which ensures that the pair be in the $^1S_0$ state. Full kinematical similarity of the reactions allows us to assume a similar behavior of the reaction amplitudes in transitions with the same set of quantum numbers of the initial proton pair and the final pion in both reactions. Zero spin of the final nucleon pair significantly simplifies the analysis of reaction (2) [27]; in particular, the number of the allowed transitions is reduced as compared with (1): the production of pion waves with odd angular momentum is forbidden, only ^3P_2d is kept from the three resonant transitions observed in reaction (1). Nevertheless, the $^3P_0$ transition forbidden in reaction (1) becomes allowed in reaction (2). In spite of these advantages of reaction (2), its experimental study was incomparably less extensive than of (1) due to a smaller cross section and necessity of high momentum resolution for the $^1S_0$ diproton identification. The proton-beam energy of $T_p = 425$ MeV in the WASA (Wide-Angle Shower Apparatus) experiment [28] was the highest for reaction (2) until the ANKE measurements from 353 to 1970 MeV were published [29–31]. The whole $\Delta(1232)$ excitation region has been scarcely explored yet.

In the present paper the first analyzing power data for reaction (2) in the $\Delta(1232)$ excitation region are presented; previous measurements of the differential cross section are complemented by additional points at 500 and 550 MeV, and the data at 700 and 800 MeV were taken additionally with higher statistics and precision: at 700 MeV the statistics increased by more than an order of magnitude, while at 800 MeV it nearly doubled, and the uncertainty of momentum reconstruction decreased by about a factor of 1.5 at both energies.

A goal of the paper is to describe the new measurements of reaction (2) and to analyze all available data on this reaction in the $\Delta(1232)$ excitation energy region.

II. MEASUREMENTS

The measurements were carried out by using the ANKE (Apparatus for Studies of Nucleon and Kaon Ejectiles) spectrometer [32] at the Cooler Synchrotron (COSY) Jülich storage ring. A schematic drawing of the experiment is shown in Fig. 2. The new data were taken during the accelerator run with the unpolarized proton beam at 353, 500, and 550 MeV energy and the two runs with the polarized proton beam, first at 500, 550, and 700 MeV, second at 800 MeV. Fast charged particles produced in the interaction of the stored proton beam with a hydrogen cluster-jet target and passing through the analyzing magnetic field were recorded in the forward detector. It includes multiwire gas chambers for tracking and a scintillation counter hodoscope for energy loss and timing measurements.

The three-momenta and trajectories of the particles were reconstructed by using the known field map of the analyzing magnet and assuming a point-like source situated at the center of the target-beam interaction volume.

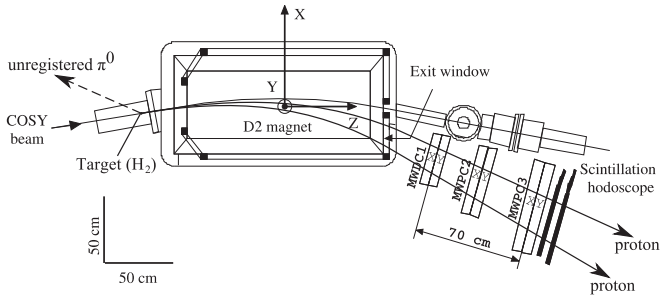

FIG. 2. The ANKE spectrometer setup (top view), showing the positions of the hydrogen cluster-jet target and the forward detector (FD).

For identification of reaction (2), proton pairs were selected first. The scintillation counter hodoscope allows measuring the difference Δt in the time of flight of both particles from the interaction point to the detector with the typical resolution less than 1 ns (rms). The time-of-flight difference can also be calculated by using the measured momenta and trajectories of the particles with their masses being assumed. In case of a proper assumption both Δt values should coincide. This allowed clean separation of pp pairs from $p\pi^+$, $d\pi^+$ pairs and the accidental coincidence background of 1% [29].

After selecting the candidates for the $pp \to ppX$ reaction, information about the momenta of both final protons allows complete kinematics of the process to be reconstructed on an event-by-event basis. The rms resolution in the diproton excitation energy E_{pp} was 0.1–0.6 MeV at $E_{pp} < 3$ MeV and provided a reliable cut in E_{pp}.

A missing-mass spectrum of the $pp \to \{pp\}_s X$ process with the M_X rms resolution of 6–40 MeV/c^2 depending on the T_p value ensured reliable separation of the pion peak from the two-pion continuum and the low-intensity γ peak [33,34]. The angular acceptance of the setup allowed registration of the diprotons at the forward angles from 0° to 24°–120° in the reaction center of mass system (c.m.s.) at different energies. The rms resolution in the polar angle θ_{pp} ranged from 0.2° to 1°, depending on T_p and θ_{pp}.

The two-dimensional registration efficiency for the pp pairs depending on their E_{pp} and θ_{pp} was determined by Monte Carlo simulations with an uncertainty of about 3%. This took into account the geometry of the setup and the sensitive areas of the detectors, the efficiency of the multiwire proportional chambers, and the track reconstruction algorithm.

The numbers of selected events for reaction (2) were then corrected on an event-by-event basis for efficiency, dead time, and, for measurements with the polarized beam, relative luminosity $L_\uparrow/L_\downarrow$ for opposite beam polarizations.

The integral luminosity was measured by using pp elastic scattering and the $pp \to d\pi^+$ reaction, both recorded concurrently with the reaction under study. The accuracy of the luminosity determination at each energy was estimated to be 7%. It includes the uncertainty of the SAID [10] prediction for differential cross sections used for normalization and the uncertainty of the registration efficiency.

The analyzing power A_y was measured with a transversely polarized proton beam repeatedly flipping the polarization direction between up and down. For the energies in the 353–700 MeV range the beam polarization was determined via the measurement of the $pp \to pp$ and $pp \to d\pi^+$ asymmetries normalized by the SAID solutions. The results gave the average value close to 0.68 ± 0.03. For the 800 MeV energy only the $pp \to pp$ channel was used, and the experimental data [36–38] were selected for normalization. This measurement resulted in the polarization of 0.57 ± 0.01.

A more detailed description of the setup, measurements, and data processing can be found in Refs. [29–34]. The only essential change in the data processing was more careful tuning of the geometry of the setup and introduction of a kinematical fit into this procedure. It allowed the systematic errors of the cross section to be notably decreased in comparison with the previous results [30].

III. EXPERIMENTAL RESULTS

Figure 3 shows the data obtained in the 353–800 MeV region. The A_y values at 353 MeV are from Ref. [31], the $d\sigma/d\Omega$ data at 353 (800) MeV are the new and Ref. [31] ([30]) data combined. The 800 MeV data published in Ref. [30] were re-analyzed by using the improved processing procedure

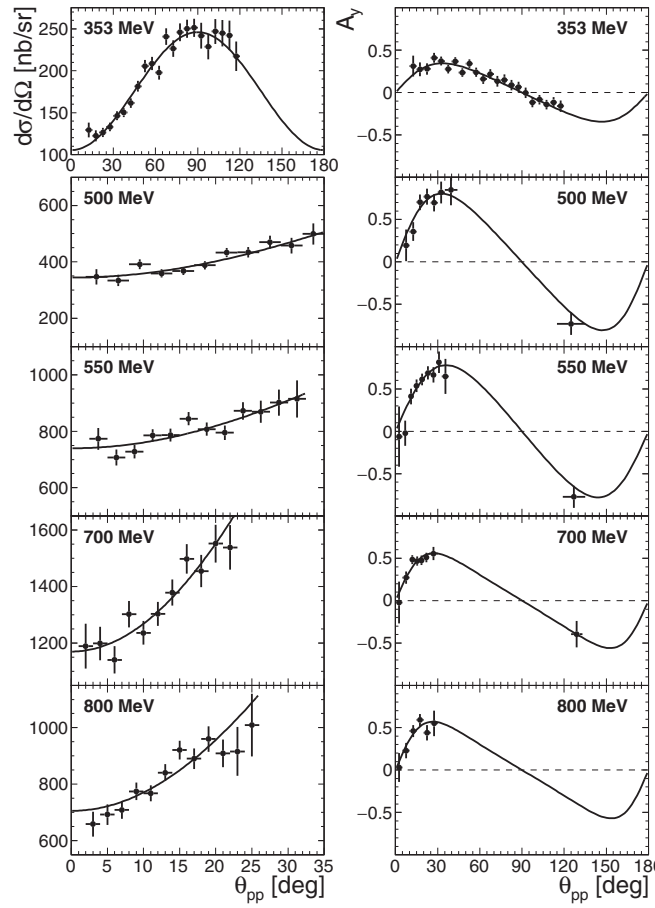

FIG. 3. Angular dependencies of the differential cross section $d\sigma/d\Omega$ (left) and the analyzing power A_y (right) at the beam energies T_p equal to 353, 500, 550, 700, 800 MeV. The errors shown are purely statistical. The curves represent fitting equations (4) to the data. See supplemental material [35] for the numerical values of $d\sigma/d\Omega$ and A_y.

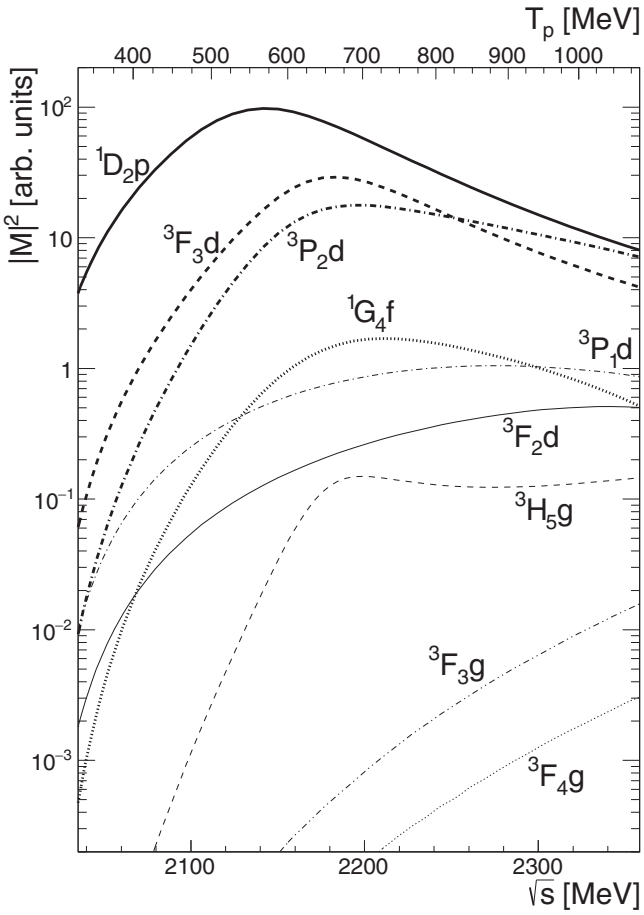

FIG. 4. Energy dependence of the leading amplitudes squared for reaction (1) according to the SAID SP96 [10] PWA calculations.

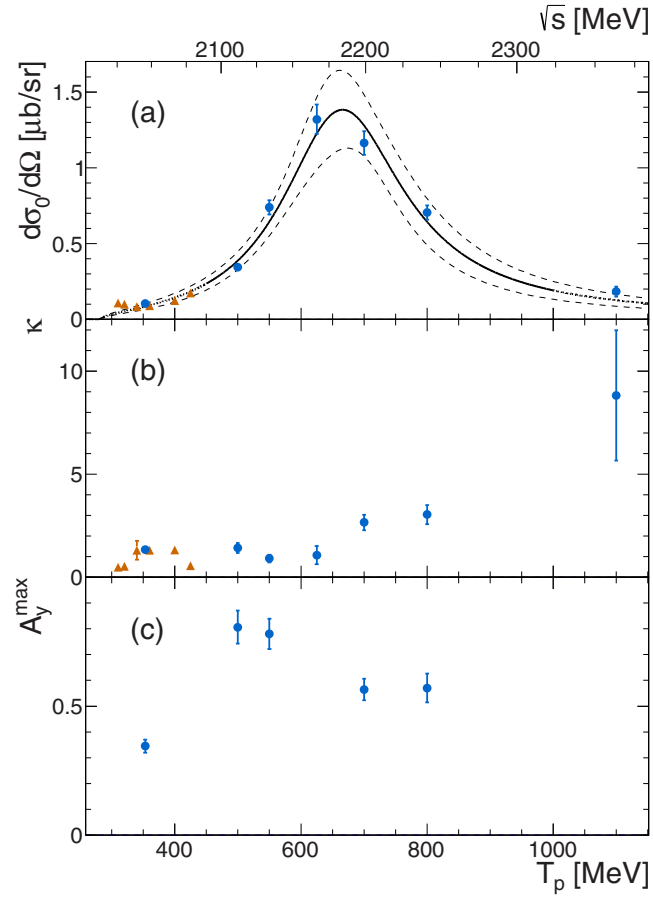

FIG. 5. Energy dependencies of the parameters fitted for $d\sigma/d\Omega$ and A_y: (a) forward cross section $d\sigma_0/d\Omega$, (b) slope parameter κ, (c) maximal analyzing power $A_y^{\max}$. ●—ANKE data (combined analysis of Refs. [30,31] and present work), ▲—WASA data [28]. The errors include statistical and systematic uncertainties from the normalization used to find luminosity and polarization. The curve approximating $d\sigma_0/d\Omega$ is the Breit–Wigner fit in the range where the line is solid. The corridor shows the 68% confidence interval.

mentioned above. The curves are a simultaneous fit of the relations

$$\frac{d\sigma}{d\Omega} = (a_0 + a_2 \cos^2\theta_{pp}),$$
$$A_y \frac{d\sigma}{d\Omega} = b_2 \sin\theta_{pp} \cos\theta_{pp} \qquad (3)$$

to the data at each energy. The relations are valid for the pion angular momentum ℓ equal to 0 and 2 [31]. The χ^2/ndf values (where "ndf" stands for "number of degrees of freedom") of the fit are in the 0.5–1.5 range.

Contribution of the next-higher angular momentum $\ell = 4$ is not visible within the obtained statistical accuracy and due to the relatively narrow angular acceptance of the ANKE forward detector. So the main justification of the restriction $\ell < 4$ comes from a comparison of reactions (1) and (2). Indeed, as is seen from Fig. 4, a square of the largest amplitude with $\ell = 4$, $|M(^3H_5g)|^2$, for reaction (1) is less than $0.02|M(^3P_2d)|^2$ in the whole energy region of interest.

Formulas (3) can be rewritten in another parametrization:

$$\frac{d\sigma}{d\Omega} = \frac{d\sigma_0}{d\Omega}(1 + \kappa \sin^2\theta_{pp}),$$
$$A_y = \frac{A_y^{\max}\sqrt{1+\kappa}\sin 2\theta_{pp}}{1 + \kappa \sin^2\theta_{pp}}, \qquad (4)$$

where $d\sigma_0/d\Omega$ means $d\sigma/d\Omega$ at the zero angle, $\kappa = a_2/a_0$ is a slope parameter, and $A_y^{\max}$ is the maximal value of A_y acquired when $\sin^2\theta_{pp} = 1/(2+\kappa)$. The energy dependencies of those parameters are shown in Fig. 5, where the $d\sigma_0/d\Omega$ and κ values from the earlier published data [28,30] are included as well. The values of the parameters are presented in Table I.

The cross section $d\sigma_0/d\Omega$ reveals a clean peak around 660 MeV. The main part of the peak was fit by the simplest Breit–Wigner form with the phase space correction. A mean value of the corresponding resonance mass, $E_P = 2181 \pm 2$ MeV, is close to the sum of a nucleon and $\Delta(1232)$ baryon masses, 2170 MeV. The width of the resonance $\Gamma_P = 101 \pm 7$ MeV is similar to the width of the free $\Delta(1232)$, 117 ± 3 MeV [39]. This suggests a possible resonance of the $N\Delta(1232)$ system which could be called a two-baryon resonance.

The angular dependence of the differential cross section has a minimum at zero degrees. It is compatible with the WASA results [28] at low energies, where the minimum was

TABLE I. The parameters of Eq. (4) fitted for $d\sigma/d\Omega$ and A_y. The sources of errors are the same as in Fig. 5.

T_p [MeV]	$d\sigma_0/d\Omega$ [μb/sr]	κ	$A_y^{\max}$
	ANKE		
353	0.105 ± 0.007	1.34 ± 0.09	0.35 ± 0.03
500	0.34 ± 0.02	1.5 ± 0.2	0.81 ± 0.06
550	0.74 ± 0.05	0.91 ± 0.18	0.78 ± 0.06
625	1.32 ± 0.10	1.1 ± 0.4	
700	1.16 ± 0.08	2.7 ± 0.4	0.56 ± 0.04
800	0.71 ± 0.05	3.0 ± 0.5	0.57 ± 0.06
1100	0.18 ± 0.03	8.8 ± 3.2	
	WASA [28]		
310	0.109 ± 0.013	0.49 ± 0.02	
320	0.102 ± 0.014	0.54 ± 0.13	
340	0.086 ± 0.018	1.3 ± 0.5	
360	0.091 ± 0.011	1.31 ± 0.08	
400	0.124 ± 0.016	1.33 ± 0.14	
425	0.17 ± 0.02	0.56 ± 0.08	

TABLE II. The parameters of Eq. (5) fitted for $d\sigma/d\Omega$ and A_y. The sources of errors are the same as in Fig. 5.

$\sqrt{s}$ [MeV]	T_p [MeV]	$\lvert M_d^P\rvert^2$	$\lvert M_s^P\rvert^2$	ϕ [deg]
		ANKE		
2045.4	353	1.43 ± 0.19	5.5 ± 0.6	145 ± 2
2111.8	500	10.6 ± 2.0	10.7 ± 1.0	128 ± 3
2133.9	550	16.1 ± 2.8	18.3 ± 1.8	121 ± 3
2166.6	625	22.7 ± 5.3	34.3 ± 5.6	125 ± 7
2198.9	700	29.1 ± 4.2	47.3 ± 4.5	146 ± 3
2241.1	800	19.8 ± 3.1	30.0 ± 2.9	148 ± 4
2363.4	1100	7.2 ± 1.8	12.4 ± 1.9	180 ± 12
		WASA [28]		
2025.6	310	0.31 ± 0.05	6.2 ± 0.9	
2030.3	320	0.30 ± 0.12	5.2 ± 0.8	
2039.5	340	1.1 ± 0.5	4.8 ± 0.8	
2048.7	360	1.08 ± 0.18	4.5 ± 0.7	
2066.9	400	1.5 ± 0.3	5.2 ± 0.8	
2078.2	425	0.43 ± 0.12	5.2 ± 0.8	

explained as a result of the s and d pion wave interference. A prominent feature of our data is the existence of this minimum at all energies. The angular slope parameter varies slowly from the near-threshold region up to 800 MeV. Another remarkable feature of the data is a significant analyzing power reaching a value of 0.8 for the energies of 500 and 550 MeV.

IV. PHENOMENOLOGICAL ANALYSIS AND DISCUSSION

The lowest initial proton states for reaction (2) are $^3P_0$, $^3P_2$, and $^3F_2$. The states of angular momenta $L \geqslant 5$ can be neglected, in similarity with reaction (1), as was pointed out above (see also Fig. 4). The ^1D_2p, ^3F_3d, ^1G_4f, and ^3P_1d transitions are forbidden for (2) because of angular-momentum and parity conservation. Consequently, only three possible transitions contribute: $^3P_0 \to {}^1S_0s$ $(J^P = 0^-)$, $^3P_2 \to {}^1S_0d$ (2^-), and $^3F_2 \to {}^1S_0d$ (2^-) with the corresponding amplitudes denoted as M_s^P, M_d^P, and M_d^F.

The $M_d^F(2^-)$ amplitude may be assumed to be considerably smaller than $M_d^P(2^-)$ and nonresonant. It is justified by the relative smallness of this amplitude at 353 MeV where the PWA [31] resulted in $|M_d^F|^2/|M_d^P|^2 = 0.045 \pm 0.026$. SAID PWA [10] gives $|M_d^F|^2/|M_d^P|^2 = 0.16$ for reaction (1) at this energy and significantly less, 0.014, for the resonance energy, 680 MeV, as is seen Fig. 4. Therefore, it is reasonable to restrict reaction (2) in this region to only two considerable amplitudes, M_s^P and M_d^P. Then, following Ref. [31] for the partial-wave decomposition and Ref. [40] for the phase space factor, one gets

$$\frac{d\sigma}{d\Omega} = \frac{(\hbar c)^2}{64\pi^2 s}\frac{k}{p}\left[\left(|M_s^P|^2 + \frac{4}{3}|M_s^P||M_d^P|\cos\phi + \frac{4}{9}|M_d^P|^2\right) + \left(-2|M_s^P||M_d^P|\cos\phi - \frac{1}{3}|M_d^P|^2\right)\sin^2\theta_{pp}\right],$$

$$A_y\frac{d\sigma}{d\Omega} = \frac{(\hbar c)^2}{64\pi^2 s}\frac{k}{p}|M_s^P||M_d^P|\sin\phi\sin 2\theta_{pp}, \quad (5)$$

where ϕ is the relative phase of the two amplitudes, s is the c.m.s. energy squared, p is the incident c.m.s. momentum, and k is the momentum of the produced pion. The $|M_s^P|$, $|M_d^P|$, and ϕ values can be determined (5) by fitting to the available $d\sigma/d\Omega(\theta_{pp})$ and $A_y(\theta_{pp})$ experimental data. At several energies below 425 MeV the cross sections measured at WASA [28] were used in the fit and, since at these energies A_y has not been measured, the $|M_d^P|^2$, $|M_s^P|^2$ values were found by fixing the relative phase ϕ with that of the $pp \to pp$ scattering, in accordance with the Watson theorem [41]. For this aim the pp-elastic-transition phases were taken by SAID [10]. At the energy of 625 MeV, the analyzing power was not measured either, so it was obtained by interpolating the results at adjacent energies, $A_y^{\max} = 0.69 \pm 0.03$.

The results of the fit are presented in Fig. 6 and Table II. The points at 400 and 425 MeV remarkably deviate from the smooth energy dependence, which can be explained by the evident nonapplicability of the Watson theorem far the reaction threshold. For this reason those points were not used in the subsequent analysis.

Figure 6 shows that both amplitudes are of a similar size and have resonance-like behavior. The M_d^P amplitude corresponds to the known $^3P_2d(2^-)$ resonance and therefore should have a fast change of its phase in the resonance region. The relative phase ϕ changes rather little (121°–148°) in the 450–800 MeV region, so the $^3P_0s(0^-)$ amplitude is well correlated with $^3P_2d(2^-)$ and should also have a rapid resonance-like phase change. So the M_s^P amplitude may be considered resonant on the same basis as M_d^P. As a result, the observed peak in the reaction differential cross section and the zero-degree minimum in the angular distributions are the result of the coherent contribution of these two leading resonant amplitudes.

In order to describe the resonance feature of the transitions in the baryon-baryon system under study, we used the Breit–Wigner expression modified due to the proximity to the

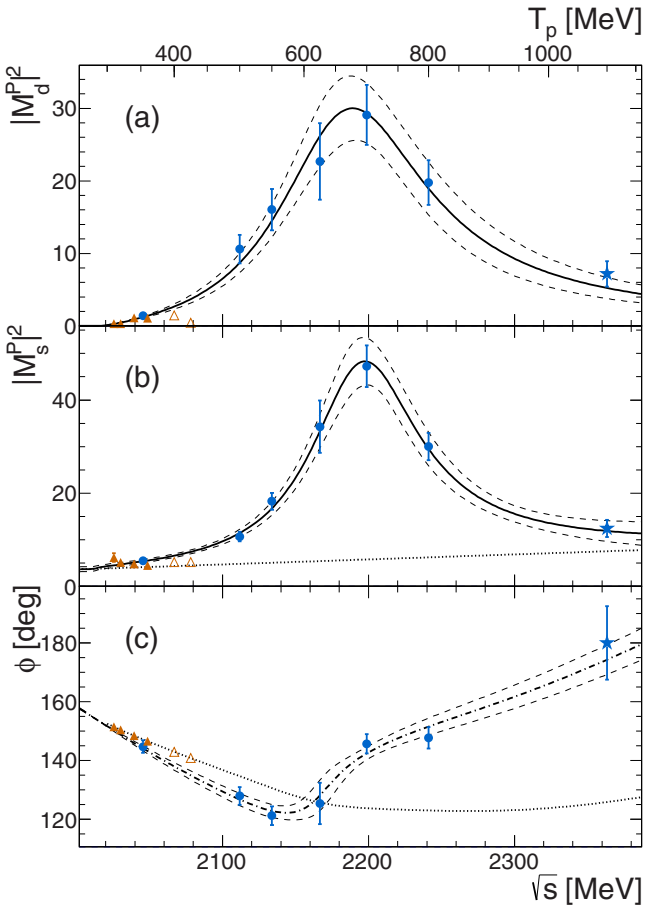

FIG. 6. Energy dependencies of the amplitudes squared of the transitions (a) ${}^3P_2 \to {}^1S_0 d$, (b) ${}^3P_0 \to {}^1S_0 s$, and (c) their relative phase ϕ. The solid curves show the approximation of the $|M_d^P|^2$ values by Eq. (6) in panel (a) and of the $|M_s^P|^2$ values by the sum of resonance (6) and background (7) in panel (b). The dash-dotted curve in panel (c) presents the approximation of the ϕ values by Eq. (8). The corridors show the 68% confidence interval. The experimental data are marked as in Fig. 5. Stars at the beam energy $T_p = 1100$ MeV correspond to the results of the fit by using $|M_d^P|^2$ extrapolation and $d\sigma/d\Omega$ data [30], as described in the text. Empty triangles are excluded from the fit for the reason given in the text. The sources of errors are the same as in Fig. 5. The dotted line in panel (b) shows the background (7). The dotted curve in panel (c) shows the relative phase of the ${}^3P_0$ and ${}^3P_2$ amplitudes in the $pp \to pp$ scattering.

reaction energy threshold:

$$|M|^2 = \frac{|M_R|^2 \Gamma \Gamma_R/4}{(\sqrt{s} - E_R)^2 + \Gamma^2/4},$$
$$\Gamma = \Gamma_R \left(\frac{k}{k_R}\right)^{2\ell+1} \frac{B_\ell(k_R)}{B_\ell(k)}, \qquad (6)$$

where M is a partial-wave amplitude, E_R is the mass of the two-baryon resonance, and Γ is the energy-dependent width, while M_R and Γ_R are the values of M and Γ at $\sqrt{s} = E_R$. The centrifugal-barrier effect was employed by the Blatt–Weisskopf penetration factor model [42,43] for a pion orbital momentum ℓ, a c.m.s. momentum k, and a characteristic radius of the pion emission volume r; k_R is the value of k at $\sqrt{s} = E_R$. Here, $B_2(k) = 9 + 3(kr)^2 + (kr)^4$, $B_0(k) = 1$.

The results for the amplitude squared $|M_d^P|^2$ depend on the factor r, unknown from an independent source and treated here as a free parameter. A fit of the $|M_d^P|^2$ dependence on energy by formula (6) [Fig. 6(a)] resulted in $|M_R|^2(2^-) = 29.5 \pm 3.5$, $E_R(2^-) = 2197 \pm 8$ MeV, $\Gamma_R(2^-) = 130 \pm 21$ MeV, and $r = 5.3 \pm 0.7$ fm with $\chi^2/\text{ndf} = 8.4/6$. The obtained parameters of the ${}^3P_2 d$ resonance practically coincide with those found in the SAID solution S96 for reaction (1): $E_R(2^-)|_{d\pi^+} = 2192$ MeV, $\Gamma_R(2^-)|_{d\pi^+} = 127$ MeV.

The $|M_s^P|^2$ distribution [Fig. 6(b)] looks like a resonance enhancement above a noticeable background. Description of the resonance essentially depends on the behavior of the background at higher energies. It is unclear there because we have no points gained from measurement of both the differential cross section and the analyzing power at beam energies above 800 MeV; note that the star points in Fig. 6 at 1100 MeV are found with a different procedure, which is described below. This procedure uses essentially the unpolarized differential-cross-section measurement at this energy [30]. The measurement shows that the cross section at this energy follows well the resonance-like energy dependence in the whole $\Delta(1232)$ excitation region and is relatively small [Fig. 5(a)]. It indicates the absence of a strong increase of a nonresonant background at this energy. On the other side, a relative smallness of the high angular-momentum amplitudes in the $\Delta(1232)$ energy region is still conserved at 1100 MeV, as is seen in Fig. 4. Therefore, it is reasonable to use the two-amplitude approach there on the same footing as in the entire Δ excitation region. Then, the differential cross section at this energy can be considered also as a result of interference between M_d^P and M_s^P amplitudes with contribution of a relatively low background. If one determines a value of the resonance amplitude M_d^P by its Breit–Wigner description with $|M_d^P|^2 = 5.2 \pm 1.5$ at 1100 MeV [Fig. 6(a)], one can find the second, M_s^P, amplitude, by fitting the differential cross section by relation (5) with $|M_s^P|^2$ and ϕ taken as free parameters. The obtained values, as well as the $|M_d^P|^2$ quantity used in this fit as a random variable, are shown by the star points in Figs. 6(a)–6(c). It is seen that the use of this fitting essentially restricts a possible background at the high side of the $|M_s^P|^2$ energy-dependence peak. A strong dominance of the resonance in this amplitude justifies a linear approximation for the background under the peak. Fit of the $|M_s^P|^2$ energy dependence by the sum of the Breit–Wigner form (6) and the background

$$\left|M_s^P\right|^2_{\text{bg}} = a_{\text{bg}} + b_{\text{bg}}(\sqrt{s} - E_R) \qquad (7)$$

resulted in $|M_R|^2(0^-) = 42 \pm 4$, $E_R(0^-) = 2201 \pm 5$ MeV, $\Gamma_R(0^-) = 91 \pm 12$ MeV, $a_{\text{bg}} = 5.8 \pm 1.3$, and $b_{\text{bg}} = 0.011 \pm 0.007$ with $\chi^2/\text{ndf} = 7.6/6$.

It is worth noting that

(i) the mass of the 0^- resonance is equal to the mass of the 2^- resonance within the 0.4% accuracy;

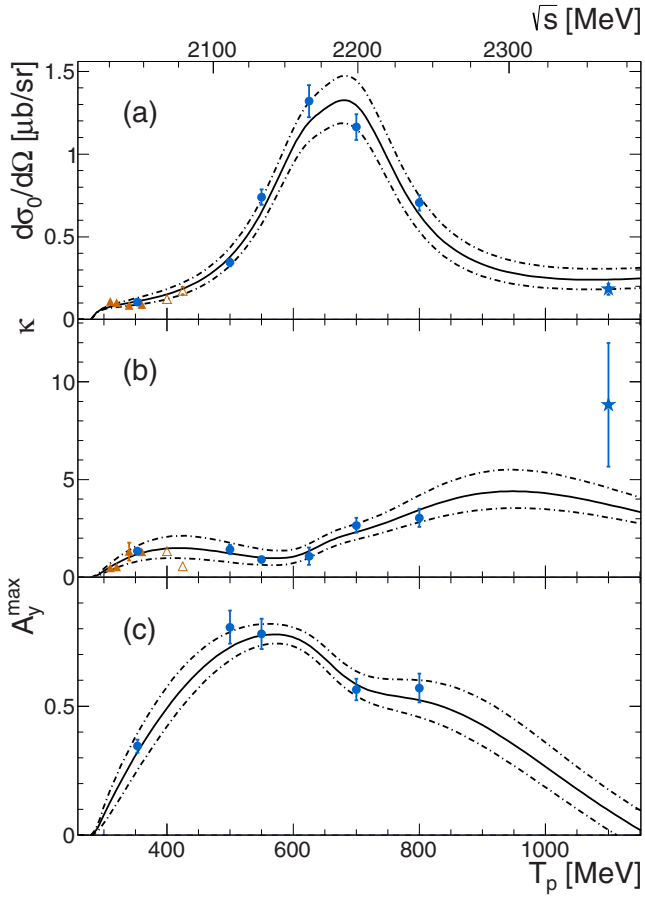

FIG. 7. Contribution of the ^3F_2d wave amplitude to the two-amplitude (^3P_0s, ^3P_2d) model calculations. Dash-dotted curves show maximal upper and lower deviations of the calculated (a) $d\sigma_0/d\Omega$, (b) κ, and (c) $A_y^{\max}$ caused by the presence of the ^3F_2d wave amplitude, as described in the text. Solid curves correspond to the results of the calculation without the ^3F_2d wave. The experimental data are marked as in Fig. 6.

(ii) the width of the 0^- resonance is slightly less than that of the free $\Delta(1232)$ isobar, $\Gamma(0^-)/\Gamma(\Delta) = 0.78 \pm 0.11$, although is compatible with it within the errors;

(iii) the phase difference ϕ between the M_s^P and M_d^P wave amplitudes found at 1100 MeV is close to 180°, which leads to the expectation of the zero analyzing power at this energy.

The $^3P_0s(0^-)$ resonance has not been observed earlier: the relevant transition is forbidden in reaction (1) and the $pp \to pp$ database is most likely not sensitive enough to this resonance because of its small branching ratio into the elastic channel. However, a recent analysis [44] of several realistic NN interactions has indicated possible existence of the $^3P_0$ resonance alongside with the known $^1D_2$, $^3F_3$, and $^3P_2$ resonances.

No phenomenological approach to describe the energy dependence of ϕ is known, so all points except the ones at 400 and 425 MeV were described by the empirical formula

$$\phi = \phi_{pp} + \frac{\sqrt{s} - \sqrt{s_0}}{p_0}\left(p_1 + \operatorname{atan}\frac{\sqrt{s} - p_2}{p_3}\right), \qquad (8)$$

where ϕ_{pp} is the energy dependent relative phase of the $^3P_0$ and $^3P_2$ amplitudes in the pp elastic scattering [10], $\sqrt{s_0} = 2013$ MeV is the reaction threshold energy, and $p_3 = 20$ MeV is fixed. The obtained values of the free parameters of the fit are $p_0 = 760 \pm 90$ MeV, $p_1 = 16^\circ \pm 11^\circ$, and $p_2 = 2169 \pm 9$ MeV.

The two-amplitude approach used here quite satisfactorily describes the full set of our experimental data (solid lines in Fig. 7). A possible deviation of the calculation caused by the presence of the third, ^3F_2d wave amplitude M_d^F, was estimated by addition of this amplitude with the $|M_d^F|^2/|M_d^P|^2$ ratio according to that for reaction (1) from the PWA (Fig. 4). The relative phase was varied in the whole interval 0°–360°. Maximum deviations of the calculated $d\sigma_0/d\Omega$, κ, and $A_y^{\max}$ from their values in the two-amplitude approach are shown in Fig. 7 by the dash-dotted curves. Relative smallness of the deviations confirms that the contribution of the F-wave amplitude can be neglected.

Analysis of reaction (2) in the frame of the three-amplitude approach was performed earlier in Ref. [45]. That calculation also used the amplitudes with the angular momenta of the initial proton pair $L \leqslant 3$ and of the pion wave $l < 4$, but the relative values of the amplitudes found there in the coupled-channels approach [46] substantially differ from ours. The M_d^P and M_d^F amplitudes were determined to be of about the same size and the M_s^P was noticeably smaller. The calculation result completely disagrees with our experimental data which was visible already in comparing it with our earlier results [30]: the calculation did not reproduce the observed significant peak in the forward differential cross section and the slope parameter greatly overestimated the experimental one. The expected striking energy dependence of the cross section also is not seen in our experiment.

The earlier described several-step procedure of the amplitude determinations can be cross-checked by an alternative calculation: a global fit. For this aim, all our experimental data on the analyzing power and the differential cross section, including 1100 MeV data, were simultaneously fit by

TABLE III. The parameters of the resonances obtained in the current analysis.

	$\lvert M_R\rvert^2$	E_R [MeV]	Γ_R [MeV]	r [fm]	$a_{\rm bg}$	$b_{\rm bg}$ [MeV^{-1}]	χ^2/ndf
$^3P_2d(2^-)$	29.5 ± 3.5	2197 ± 8	130 ± 21	5.3 ± 0.7			8.4/6
$^3P_0s(0^-)$	42 ± 4	2201 ± 5	91 ± 12		5.8 ± 1.3	0.011 ± 0.007	7.6/6
$^3P_2d(2^-)$[a]	28.1 ± 3.5	2207 ± 12	170 ± 32	4.4 ± 0.3			304/277
$^3P_0s(0^-)$[a]	41 ± 3	2204 ± 4	95 ± 9		6.2 ± 0.8	0.012 ± 0.004	304/277

[a]The results of the global fit.

TABLE IV. Fit results for the amplitudes squared $|M_d^P|^2$ and $|M_s^P|^2$ and the phase angle ϕ at 1100 MeV energy.

	$\lvert M_d^P\rvert^2$	$\lvert M_s^P\rvert^2$	ϕ [deg]
Step-by-step fit	7.2 ± 1.8	12.4 ± 1.9	180 ± 12
Global fit	7.5 ± 1.7	12.7 ± 1.5	180 ± 15

employing Eqs. (5)–(7). The free parameters of this fit were ϕ at every available energy, $|M_R|^2$, E_R, and Γ_R for each of the two resonances, and r, $a_{\rm bg}$, and $b_{\rm bg}$. The solution of this global fit is presented in Table III together with the results of the several-step procedure. The output of the both agree within the errors. Particular results for the amplitudes squared and the phase angle at 1100 MeV energy are given in Table IV. They also confirm compatibility of the analysis results.

The energy position of the resonances can be qualitatively interpreted by assuming a resonance in the P-wave state of the ΔN pair. In the absence of the ΔN interaction and relative motion its mass is a sum of the Δ and nucleon masses, that is, 2170 MeV/c^2. The orbital P-wave motion should increase the invariant mass by about 60 ± 7 MeV/c^2, as it takes place for the P wave of the ΔN intermediate state as compared to its S-wave state in reaction (1) [9,10]. Thus, the mass should be 2230 ± 7 MeV/c^2. The difference between this value and the observed one is 29 ± 9 MeV/c^2 for 0^- and 33 ± 11 MeV/c^2 for 2^- resonances. This indicates a strength of the attraction in the intermediate P-wave ΔN pair.

A quantitative description of the obtained results requires relevant model calculations using hadronic or QCD degrees of freedom, as well as an interplay of both of them [21,47,48], to gain a better insight into the physical nature of the two-baryon resonance states.

V. SUMMARY

The measured differential cross section of the single-pion production with the $^1S_0$ diproton forward emission reveals a clear peak in the $\Delta(1232)$ excitation energy region. The angular dependence of the pair emission has a minimal value at zero degrees through the whole energy region studied. The analyzing power is significant, and its maximum varies 0.3 to 0.8 at different energies.

A simple model assuming significant contributions of only two amplitudes, M_s^P and M_d^P, allows us to describe all the data; in particular, it suggests a strong enhancement of both amplitudes in the Δ excitation region. The energy dependence of the amplitudes squared is well reproduced by the Breit–Wigner distribution modified by the Blatt–Weisskopf penetration factor. The parameters of the ^3P_2d resonance coincide with those known for the $pp \to d\pi^+$ reaction. The parameters of the resonance ^3P_0s are close to them. The position of the resonances indicates a noticeable attraction in the P-wave state of the intermediate ΔN pair. Our study also suggests that the diproton formation may be similarly used in the reaction $pp \to \{pp\}_s\pi\pi$ [49] as a tool for searching for isovector two-baryon-system resonances above the ΔN region [48].

ACKNOWLEDGMENTS

We are thankful to the COSY synchrotron crew for the fine conditions of the experiment. We are grateful to V. Burov and I. Strakovsky for useful discussions and to J. Złomańczuk for kindly providing us with the WASA@CELSIUS experimental data. We express a special gratitude to C. Wilkin for extensive and valuable discussions of the experiment and analysis. This work has been supported by the Forschungszentrum Jülich (COSY-FEE).

[1] R. J. Oakes, Phys. Rev. **131**, 2239 (1963).
[2] F. J. Dyson and N. H. Xuong, Phys. Rev. Lett. **13**, 815 (1964).
[3] A. Th. M. Aerts, P. J. G. Mulders, and J. J. de Swart, Phys. Rev. D **17**, 260 (1978).
[4] P. J. Mulders, A. T. Aerts, and J. J. de Swart, Phys. Rev. D **21**, 2653 (1980).
[5] R. A. Arndt, L. D. Roper, R. A. Bryan, R. B. Clark, B. J. VerWest, and P. Signell, Phys. Rev. D **28**, 97 (1983).
[6] R. A. Arndt, J. S. Hyslop, and L. D. Roper, Phys. Rev. D **35**, 128 (1987).
[7] R. A. Arndt, W. J. Briscoe, I. I. Strakovsky, and R. L. Workman, Phys. Rev. C **76**, 025209 (2007).
[8] B. G. Ritchie, Phys. Rev. C **28**, 926 (1983).
[9] R. A. Arndt, I. I. Strakovsky, R. L. Workman, and D. V. Bugg, Phys. Rev. C **48**, 1926 (1993).
[10] SAID interactive code, http://gwdac.phys.gwu.edu
[11] J. A. Niskanen, Nucl. Phys. A **298**, 417 (1978).
[12] O. V. Maxwell and W. Weise, Nucl. Phys. A **348**, 429 (1980).
[13] B. Blankleider and I. R. Afnan, Phys. Rev. C **24**, 1572 (1981).
[14] J. A. Niskanen, Phys. Lett. B **141**, 301 (1984).
[15] C. Furget *et al.*, Nucl. Phys. A **655**, 495 (1999).
[16] M. Schwamb, Phys. Rep. **485**, 109 (2010).
[17] A. Gal and H. Garcilazo, Phys. Rev. Lett. **111**, 172301 (2013).
[18] V. I. Kukulin, I. T. Obukhovsky, V. N. Pomerantsev, and A. Faessler, J. Phys. G: Nucl. Part. Phys. **27**, 1851 (2001).
[19] A. Valcarce *et al.*, Rep. Prog. Phys. **68**, 965 (2005).
[20] J. L. Ping, H. X. Huang, H. R. Pang, F. Wang, and C. W. Wong, Phys. Rev. C **79**, 024001 (2009).
[21] M. N. Platonova and V. I. Kukulin, Phys. Rev. C **87**, 025202 (2013).
[22] M. Bashkanov *et al.*, Phys. Rev. Lett. **102**, 052301 (2009).
[23] P. Adlarson *et al.*, Phys. Rev. Lett. **106**, 242302 (2011).
[24] P. Adlarson *et al.*, Phys. Rev. Lett. **112**, 202301 (2014).
[25] M. Bashkanov, S. J. Brodsky, and H. Clement, Phys. Lett. B **727**, 438 (2013).
[26] M. Bashkanov, H. Clement, and T. Skorodko, arXiv:1502.07500.
[27] Yu. N. Uzikov, Phys. At. Nucl. **77**, 646 (2014).
[28] R. Bilger *et al.*, Nucl. Phys. A **693**, 633 (2001).
[29] S. Dymov *et al.*, Phys. Lett. B **635**, 270 (2006).
[30] V. Kurbatov *et al.*, Phys. Lett. B **661**, 22 (2008).
[31] D. Tsirkov *et al.*, Phys. Lett. B **712**, 370 (2012).
[32] S. Barsov *et al.*, Nucl. Instrum. Methods Phys. Res., Sect. A **462**, 364 (2001).

[33] V. Komarov *et al.*, Phys. Rev. Lett. **101**, 102501 (2008).
[34] D. Tsirkov *et al.*, J. Phys. G **37**, 105005 (2010).
[35] See Supplemental Material at http://link.aps.org/supplemental/10.1103/PhysRevC.93.065206 for the differential cross sections and analyzing power of reaction (2).
[36] M. W. McNaughton, P. R. Bevington, H. B. Willard, E. Winkelmann, E. P. Chamberlin, F. H. Cverna, N. S. P. King, and H. Willmes, Phys. Rev. C **23**, 1128 (1981).
[37] F. Irom, G. J. Igo, J. B. McClelland, and C. A. Whitten, Phys. Rev. C **25**, 373 (1982).
[38] G. Pauletta *et al.*, Phys. Rev. C **27**, 282 (1983).
[39] Particle Data Group, K. A. Olive *et al.*, Chin. Phys. C **38**, 090001 (2014).
[40] Yu. N. Uzikov, Fiz. Elem. Chastits At. Yadra **29**, 1405 (1998) [Phys. Part. Nucl. **29**, 583 (1998)].
[41] K. M. Watson, Phys. Rev. **88**, 1163 (1952); A. B. Migdal, Sov. Phys. JETP **1**, 2 (1955).
[42] F. von Hippel and C. Quigg, Phys. Rev. D **5**, 624 (1972).
[43] D. J. Herndon *et al.*, Phys. Rev. D **11**, 3183 (1975).
[44] G. Papadimitriou and J. P. Vary, Phys. Lett. B **746**, 121 (2015).
[45] J. A. Niskanen, Phys. Lett. B **642**, 34 (2006).
[46] J. A. Niskanen, Phys. Rev. C **49**, 1285 (1994).
[47] A. Gal and H. Garcilazo, Nucl. Phys. A **928**, 73 (2014).
[48] M. N. Platonova and V. I. Kukulin, Nucl. Phys. A **946**, 117 (2016).
[49] S. Dymov *et al.*, Phys. Rev. Lett. **102**, 192301 (2009).